Cold Regions Science and Technology 200 (2022) 103587

Contents lists available at ScienceDirect

Cold Regions Science and Technology

journal homepage: www.elsevier.com/locate/coldregions

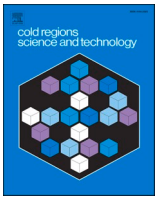

Exploring snow distribution dynamics in steep forested slopes with UAV-borne LiDAR

Kalliopi Koutantou [a,b,*], Giulia Mazzotti [b], Philip Brunner [a], Clare Webster [b,c], Tobias Jonas [b]

[a] Centre for Hydrogeology and Geothermics (CHYN), University of Neuchatel, Neuchatel, Switzerland
[b] WSL Swiss Federal Institute for Snow and Avalanche Research SLF, Davos, Switzerland
[c] Swiss Federal Institute for Forest, Snow, and Landscape Research WSL, Birmensdorf, Switzerland

ARTICLE INFO

Keywords:
UAV
LiDAR
Snow depth mapping
Steep forests
Canopy structure
Canopy radiative transfer

ABSTRACT

Mapping snow in forests is important for understanding the snow cover dynamics in these environments in view of hydrological applications and water resources management. Today, Uncrewed Aerial Vehicles (UAVs) are widely used for snow studies due to their rather cheap and flexible operation. UAV-borne Light detection and ranging (LiDAR) systems are a promising technology for sub-canopy snow mapping at high temporal resolutions, concurrently providing information on both the canopy and the below-canopy snow surface. In this pilot study, we used a UAV-LiDAR system to investigate the snow cover dynamics within two steep forested slopes of opposing aspects in the Swiss Alps at both high spatial resolution and unprecedented temporal resolution. Using a Distance to Canopy Edge (DCE) algorithm to characterize local forest structure, snow depth was analyzed in terms of relative position within variable forest cover. The north-exposed site had higher mean snow depths throughout the season compared to the south-exposed site, especially in canopy gaps. Whereas snow depletion rate was consistent throughout the north-exposed site, snow depletion was much faster in the gaps at the south-exposed slope. Correlation coefficients between snow depths and local canopy closure were weaker at the south-exposed (between −0.5 and − 0.7) than at the north-exposed site (between −0.7 and − 0.9), and rapidly deteriorated right after the peak of winter at the south-exposed slope. This indicates shortwave radiation dominates snowmelt processes at this site, which was thought to be spatially uncorrelated to local canopy cover, unlike accumulation and melt processes on the north-exposed slope that generated snow patterns with a high spatial correlation to local canopy cover throughout the entire season. Calculations of incoming sub-canopy shortwave radiation (SWR) for both sites confirmed this assumption. While our findings encourage the use of UAV-borne LiDAR for further investigations of snow cover dynamics in steep forested slopes, we also outline and discuss technical challenges specific to this application. Our insights allow deriving useful recommendations for future studies using UAV-borne LiDAR over a similar environment.

1. Introduction

Forests cover around 30% of the surface of Switzerland (Hunziker et al., 2012), and a large extent of the Northern Hemisphere is forested and features a seasonal snow cover (Essery et al., 2009). Snowmelt runoff originating from forests has a significant impact on hydrology, ecology, and climate (Javadinejad et al., 2020). Especially in Alpine regions, numerous studies have demonstrated the effect of snow cover dynamics on water resources (Farinotti et al., 2012; Thornton et al., 2021), natural hazards such as avalanches and floods (Einhorn et al., 2015; Björk and Molau, 2007), ecology (Nöthiger and Elsasser, 2004; Wipf et al., 2009) as well as tourism (Rixen et al., 2011; Elsasser and Bürki, 2002). As forests cover large areas that overlap with seasonal snow, forest snow cover dynamics need to be represented in models simulating snow cover dynamics in these environments (Mazzotti et al., 2020b; Mazzotti et al., 2021).

Spatially heterogeneous forest canopy causes correspondingly heterogeneous accumulation and melt patterns in both space and time (Lundquist et al., 2013; Currier and Lundquist, 2018; Mazzotti et al., 2019b). Snow cover dynamics in forests are thus usually more complex than in open sites (Clark et al., 2011). Accumulation patterns are affected by snow interception by the canopy (Hedstrom and Pomeroy,

* Corresponding author at: Centre for Hydrogeology and Geothermics (CHYN), University of Neuchatel, Neuchatel, Switzerland.
E-mail address: kalliopi.koutantou@unine.ch (K. Koutantou).

https://doi.org/10.1016/j.coldregions.2022.103587
Received 25 October 2021; Received in revised form 4 April 2022; Accepted 9 May 2022
Available online 13 May 2022

1998). The intercepted snow either sublimates, melts, or falls on the below-canopy snow surface (MacKay and Bartlett, 2006). Snowmelt is driven by a combination of processes such as the turbulent exchange of heat and water and the transfer of shortwave (SWR) and longwave radiation (LWR) to the snow surface (Jonas and Essery, 2011). The existence of trees decelerates wind and interferes with the turbulence exchange of heat and moisture at the snow surface. Trees shade the snow surface from SWR (Hardy et al., 2004; Malle et al., 2019) and canopy litter on the snow surface absorb higher amounts of incoming SWR (Perrot et al., 2011). Additionally, the trees are emitters of LWR, thereby enhancing incoming LWR to the snow surface relative to non-forested areas (Hedstrom and Pomeroy, 1998; Webster et al., 2016). All these processes are strongly influenced by the local canopy structure and therefore feature complex spatiotemporal dynamics (Clark et al., 2011; Jonas and Essery, 2011). Within alpine regions, forest structure impacts on snow cover dynamics are superimposed by respective topographic effects. Therefore, the interplay of forest structure and topography must be considered for snow models to be suitable for application in Alpine countries such as Switzerland. Hence, there is a need to understand snow cover dynamics in forested slopes to develop, validate and improve existing models for these environments (Mazzotti et al., 2019a; Clark et al., 2011).

Snow mapping in Alpine and especially in steep terrain is challenging due to difficult accessibility, avalanche danger, and the frequency of rough weather conditions. Traditional in situ measurements, either manually acquired or from automatic weather stations, are largely limited to flat terrain and only representative of point locations (Bründl et al., 2004; Egli, 2008). This circumstance has triggered significant interest in modern remote sensing technologies for mapping snow distribution over continuous, large, and difficult to access areas (Kim et al., 2017). However, for snow depth mapping within forests, the use of remote sensing technology is currently still mostly limited to Light detection and ranging (LiDAR) (Mazzotti et al., 2019a; Broxton et al., 2015; Currier and Lundquist, 2018; Zheng et al., 2016; Currier et al., 2019), while other sensors (e.g. optical) cannot "see" below the canopy. The potential of LiDAR for capturing fine-scale snow patterns within forests of different canopy types and structures has previously mainly been explored and demonstrated based on Airborne Laser Scanning (ALS) data (Hopkinson et al., 2004; Currier et al., 2019; Deems et al., 2013). As an active scanning technology that operates at high frequency, where each laser pulse has a very small footprint, LiDAR can penetrate even small canopy gaps. Moreover, given its ability to record multiple returns per shot, LiDAR provides information from the canopy itself as well as from the below-canopy ground surface. These characteristics make it an ideal technology to explore how snow patterns relate to canopy structure. However, one of the major drawbacks of ALS is the fact that data acquisitions come with high costs and logistic efforts, therefore on-demand campaigns at high temporal resolution are often unfeasible. Additionally, some remaining data gaps in sub-canopy areas have been reported (Mazzotti et al., 2019a; Broxton et al., 2015; Currier and Lundquist, 2018; Zheng et al., 2016; Currier et al., 2019). These errors are enhanced by terrain-related factors such as the slope and by the presence of understory vegetation (Deems et al., 2013; Hyyppä et al., 2005; Su and Bork, 2006; Tinkham et al., 2012; Hopkinson et al., 2004). They are further influenced by survey parameters, including scanning angle, pulse density, pulse size (footprint), or the operational flying height (Deems et al., 2013; Goodwin et al., 2006; Tinkham et al., 2012). Many forests in alpine regions are located on slopes, because land-use practices have led to deforestation in most flat areas (Bebi et al., 2017). Weaknesses in ALS from crewed aircraft in collecting snow depth datasets is an impediment to the improvement of the understanding of snow cover dynamics in alpine forests.

In contrast to crewed aircraft, UAVs are cheaper and more flexible options. They enable data acquisition at higher temporal resolutions and much lower costs, however, the spatial extent they can cover is more limited. So far, UAVs have been widely used with optical sensors to map snow in open areas using photogrammetric techniques (structure from motion) for mapping snow in high resolutions (Bühler et al., 2016; Vander Jagt et al., 2015; Avanzi et al., 2018). The studies yielded satisfactory results in the open but were unable to obtain accurate below-canopy information. For forest snow mapping, UAV-borne LiDAR is a promising technology, combining the flexibility of UAVs and the capabilities of LiDAR systems. Yet, the use of UAV-borne LiDAR is only emerging: Until now, only three studies using this technology to investigate forest snow have been conducted (Harder et al., 2020; Jacobs et al., 2021; Cho et al., 2021), none of which is focused on steep terrain.

In fact, only a few studies on forest snow on steep slopes are available to date. Ellis et al. (2011) used a manually acquired dataset with high temporal resolution but only presented data from one individual site. The study exclusively focused on the snowmelt period and did not cover accumulation dynamics. Broxton et al. (2020) presented a larger dataset obtained with ALS over steep terrain, but with limited temporal resolution. Other studies investigating the relation between snow pattern evolution and canopy structure were either based on data from terrestrial laser scanners (Hojatimalekshah et al., 2021; Uhlmann et al., 2018; Zheng et al., 2018) or ALS (Mazzotti et al., 2019a; Moeser et al., 2020; Broxton et al., 2015; Trujillo et al., 2007) and were largely limited to flat forests.

This paper presents a study conducted in the European Alps, which is to the best of our knowledge the first that explores the use of repeated UAV-borne LiDAR acquisitions to investigate the full seasonal cycle of snow cover dynamics in forested slopes. The goal was to obtain a high-resolution time series of snow depth maps on two opposing (north and south-exposed) slopes and analyze these in the context of variable forest structure to characterize the snow cover dynamics of a typical alpine forest. Given the limited community experience with UAV-borne LiDAR applications, we further report our experiences with this technology, building on the insights of Harder et al. (2020) and Jacobs et al. (2021) aiming at facilitating the use of this novel technology for future snow studies in areas where forest cover and complex terrain overlap.

We present datasets acquired throughout one winter in Davos, Switzerland, focusing our analysis on:

1. A comparison of the snow accumulation and melt dynamics between the two opposing slopes.
2. The links between snow depth distribution canopy structure descriptors as well as topographic influences in steep forested slopes.
3. Evaluation of the UAV-borne LiDAR technology for mapping forest snow in complex terrain at high spatio-temporal resolution.

2. Data

2.1. Study sites

Data were collected over two forested slopes with opposing orientations in Davos Dorf, in the Swiss Alps. The south-exposed site, Wariwald, is exposed to direct insolation throughout the whole winter season. The other site, Abiwald, is oriented towards the North and thus predominately shaded. The sites are located within 400 m horizontal distance of each other, at approximately 46.810°, 9.856°, 1650 m.a.s.l. (Fig. 1). Each field site encompasses an area of heterogeneous forest of 200 by 200 m, including both dense canopy and gaps. The average slopes are 20° and 35° for Wariwald and Abiwald, respectively. The dominant tree species is spruce, with few individual larches. For ease of interpretation, the sites are referred to as Wariwald-sunny and Abiwald-shaded.

2.2. Equipment and LiDAR data acquisition

Data were acquired using a Yellowscan Mapper II LiDAR scanner mounted on a twelve-motor multicopter from Altigator SA. The UAV can lift payload up to 12 kg and maintains stability even during windy

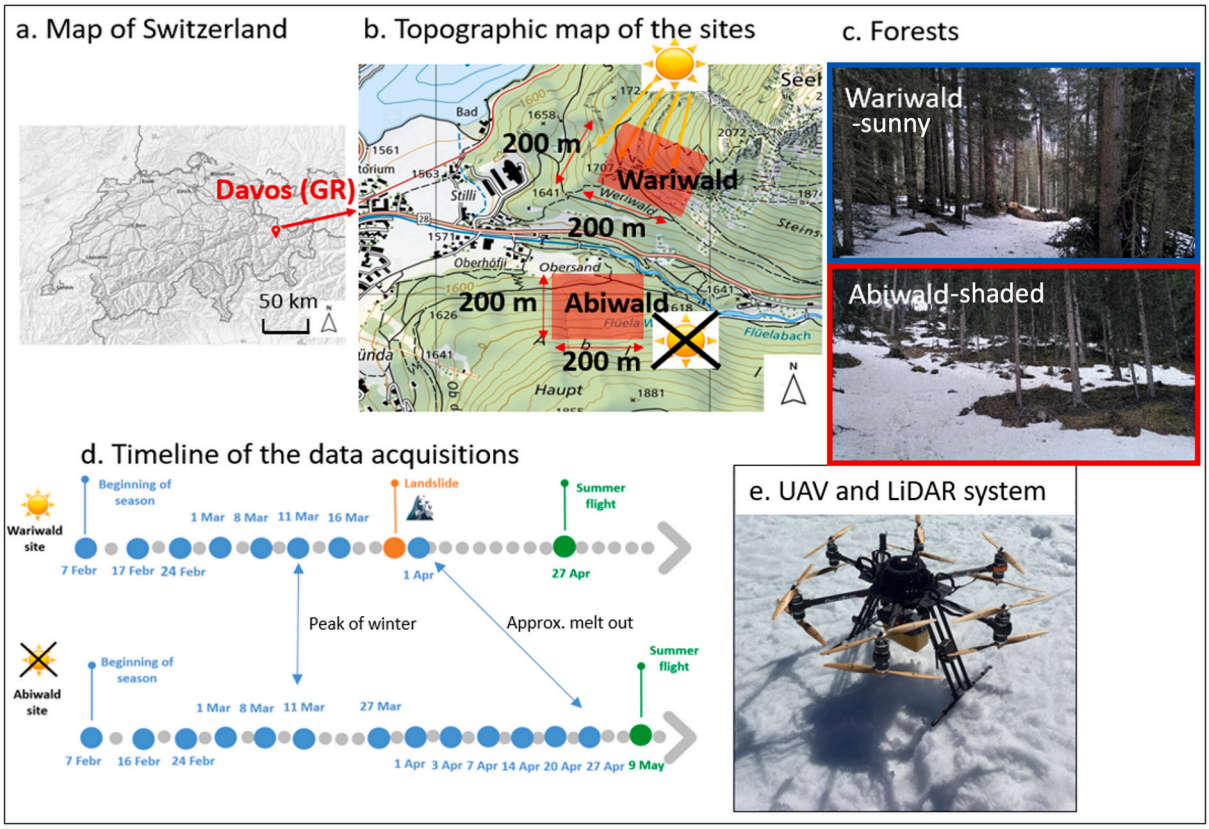

Fig. 1. The two forest slopes of our study show a) on the map of Switzerland (source: https://map.geo.admin.ch/) and b) on a topographic map (source: https://map.geo.admin.ch/); c) photographs of the forested slopes; d) timeline of the data acquisitions for both sites; e) UAV system with the LiDAR scanner.

conditions. The LiDAR scanner operates in the near-infrared range (905 nm). It has a field of view of 100°, with about 18,500 shots per second and up to three returns per shot with a precision of 10 cm. Its integrated Applanix APX-15 Inertial Navigation System (INS) offers accuracies after post-processing up to 5 cm for positioning, 0.015 m/s for velocity, 0.025 degrees for roll and pitch, and 0.080 degrees for true heading. The operation at the specific wavelength of 905 nm is suitable for retrievals of snow, given the high backscattering intensity from the canopies or the snow surface at this wavelength.

The sites were covered with four interlaced scan patterns consisting of four flight strips each (see Fig. 2), the combination of which is hereafter referred to as one acquisition. This acquisition structure was chosen to achieve a high point density, as well as to increase the sub-canopy returns by scanning the same area from different angles. The

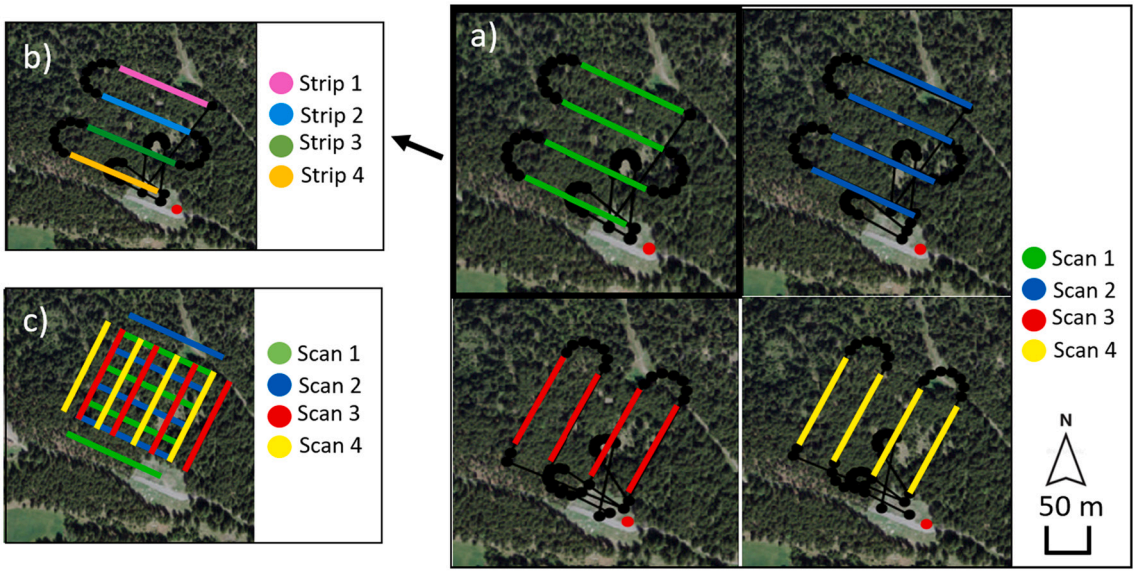

Fig. 2. Illustration of the scans and strips designed for Wariwald-sunny field site: interlaced scans (a); 4 strips of one of the scans (b), and all the four interlaced scans for one data acquisition (c).

latter is aimed at increasing the LiDAR returns from the below-canopy areas, especially in the denser parts of the forests. The flight trajectories were programmed to follow the topography, to ensure a constant elevation of 70–80 m above ground, at a constant flying speed of 3 m/s. These specific survey parameters led to an average return density of 30 points/m^2 per flying pattern.

All the flights were performed during calm weather conditions and minimal wind to reduce power consumption, to allow safe operation of the UAV, and to maximize positioning accuracy by minimizing INS drift. The flight duration was limited to approximately 13 min. The relatively short flying time was influenced by the increased power consumption at the high altitude as well as the reduced battery performance at cold temperatures. When possible, data acquisition was restricted to periods without snow intercepted by the canopy to maximize the occurrence of laser pulses penetrating the canopy.

Data acquisition commenced at the beginning of February at both sites when the seasonal snowpack began to build up. It comprised eight winter (hereafter snow-on) acquisitions over Wariwald-sunny and thirteen acquisitions over Abiwald-shaded over the same number of days (i.e. one acquisition at each site per date in Fig. 1). Summer (hereafter snow-off) acquisitions were carried out at the end of April (Wariwald-sunny) and mid-May (Abiwald-shaded). A landslide event at the end of March close to the Wariwald-sunny site inhibited further acquisitions on a regular basis, as permission to access the site was only granted for two more data acquisitions. For this reason, only limited data is available for the final snowmelt period at Wariwald-sunny compared to Abiwald-shaded. Luckily, the dataset still includes acquisitions before, at, and after the peak of winter, allowing the characterization of snow cover dynamics over the season.

2.3. Auxiliary data acquisition

Snow depth stakes were established at five locations within each of the field sites to obtain ground truth data for the LiDAR acquisitions. The selection of stake locations was constrained by accessibility, steepness of the terrain, avalanche danger, and the necessity to limit disturbance to the snow surface. Stakes were installed before the first flight in February and removed when the sites became snow-free. Snow depth at all stakes at both sites was recorded on the same day as all winter data acquisitions.

Further auxiliary data was retrieved from the meteorological station of the IMIS network (Interkantonales Mess- und Informationssystem) in Davos and the co-located snow depth measurement site. These data included hourly open-site solar radiation data used for sub-canopy radiation modeling (section 3.4), as well as daily snow depth measurements used as open-site reference values.

3. Methods

Information on both canopy characteristics and snow distribution can be extracted from LiDAR point clouds. Snow depth maps are obtained by differencing digital elevation models (DEMs) of snow-off and snow-on acquisitions, while LiDAR returns from vegetation can be rasterized into canopy height models or used as input to radiation transfer models. The following sections outline the workflows applied for these purposes.

3.1. UAV-borne LiDAR point cloud data processing

Prior to creating any gridded product, several LiDAR point cloud post-processing steps were required. These included 1) registration workflows to create optimally georeferenced point clouds, and 2) point classification algorithms to allow discriminating between snow/ground and vegetation points, used to derive the snow depths and canopy structure datasets, respectively.

3.1.1. Post-Processing kinematic correction and point cloud registration

The position and attitude recordings of the INS were merged with the raw LiDAR returns and processed to georeferenced point clouds within the licensed CloudStation software (YellowScan CloudStation, 2021). To further improve the positioning accuracy, the flight trajectory was post-processed using the data of a Global Navigation Satellite System (GNSS) base station from the continuously operating reference stations (CORS) of the Swiss positioning system (SWIPOS). The base station chosen was within approximately 1 km of the two sites. This post-processing kinematic (PPK) correction was performed using the third-party licensed software POSPac UAV (Applanix, 2019). The outcome of the PPK correction was the post-processed Smoothed Best Estimate Trajectory (SBET) that was then used for improving the geolocation of the point clouds.

The SBET-based correction of point clouds was assessed based on the alignment accuracy of the four strips for each individual scan, as illustrated in Fig. 2. For further improving alignment accuracy where necessary, we applied a manual strip adjustment workflow to neighboring strips as follows: A vertical profile in the overlapping area of the point clouds corresponding to the two strips (e.g. the orange and green lines in Fig. 2a) was considered, and one was manually registered to the other to minimize offsets between the two, where the latter one remained static as reference. The 3D transformation matrix derived from this manual registration was then applied to the whole strip.

The next step was the registration of all the four scans into one point cloud. Each individual LiDAR scan includes inaccuracies that might generate from GPS or INS drifts, the PPK correction, or during the manual adjustment of the strips of each scan. The resulting geolocation errors should be minimized by the registration of the individual scans. We applied the same manual adjustment workflow as for the strips' registration, now using the whole scans instead of individual strips. The result was one combined point cloud for each data acquisition. These combined point clouds featured return densities of approximately 120 pts. / m2. The snow-on and snow-off point clouds were not fully registered to each other, despite the numerous registration algorithms we tested (see discussions section). However, the misalignments between snow-on and snow-off point clouds were minimized through the previous steps and further fine-tuning of the so-far alignment procedure was not considered beneficial at this point.

3.1.2. Point cloud classification

The classification of each of the LiDAR point clouds into ground and non-ground points is an essential prerequisite for deriving any gridded product from the point clouds. In our case, this classification served to discriminate between returns from the snow or bare-earth surface (in snow-on and snow-off acquisitions, respectively), and returns from the vegetation (understory and trees). For snow mapping studies, a robust ground point classification is especially critical, as errors will translate into inaccuracies in snow depths. However, forested slopes represent a particularly challenging terrain for classification algorithms, as elevation differences between neighboring points can occur either because the ground is sloped, or because they belong to different classes (snow/ground or vegetation).

We used the lasground tool from LAStools software (LAStools, Academic Version 190812, 2019) that classifies points into ground and non-ground points. The most satisfying results, based on visual inspection, were obtained with the settings "step = 3m" and "offset = 1m" (for both sites). To account for any remaining noise within the classified point clouds, we performed additional filtering using the lasthin tool (LAStools). In the case of snow-on acquisition, we kept "snow points" that were between the 50th and 60th percentiles of all elevation values within a 20 cm by 20 cm horizontally moving window, similar to the approach applied in Mazzotti et al. (2019a).

In the case of the snow-off point clouds, the main challenge was the separation between bare-earth and understory vegetation points (Riaño et al., 2007; Spaete et al., 2011; Streutker and Glenn, 2006). Understory

vegetation at our sites consisted mainly of tall grasses and blueberry bushes, which are completely buried and pushed down by the snow and hence do not represent an issue during winter acquisition. However, in the case of snow-off flights, returns from understory vegetation are possible and could be misclassified as ground points, resulting in an overestimation of the elevation of the bare earth surface, and an eventual underestimation of the snow depths (Currier et al., 2019; Hopkinson et al., 2004; Tinkham et al., 2012). To minimize the occurrence of such artifacts, we slightly adapted the filtering with the lasthin tool, keeping "ground" points that were between the 40th and 50th percentiles of all elevation values within a 20 cm by 20 cm horizontally moving window.

The classified point clouds obtained with the above workflow constituted the basis for extracting snow depth grids (Fig. 3/section 3.2), as well as for producing the canopy height models and corresponding canopy structure descriptor derivatives (Fig. 4/section 3.3).

3.2. Snow depth data processing

The workflow to obtain snow depth maps is summarized in Fig. 3. Following the classification of point clouds, snow or bare-ground returns for each acquisition were rasterized into 1 m DEMs, producing maps of snow depth (snow-on DEMs) or bare-earth (snow-off DEMs) respectively. We applied the lasgrid tool (LAStools) to every individual snow-on and snow-off point cloud, where each pixel in the DEM was calculated as the average elevation of all points contained within that pixel. The resulting grids contained gaps corresponding to the below-canopy areas where no returns were captured.

To fill these gaps, we applied the procedure suggested by Mazzotti et al. (2019a) which relies on the las2dem tool from LAStools. This tool triangulates LiDAR returns by using a temporary triangulated irregular network (TIN) and then rasterizes the TIN into a grid of 1 m resolution. During the TIN creation, all triangles bigger than 10 m were discarded and these areas remained as gaps in the final DEMs. Subsequently, the las2dem-derived DEMs were used to fill the gaps in the lasgrid-derived DEMs. To remove the high-frequency noise present in the DEMs, we smoothed the DEMs by applying a 3 by 3 kernel low-pass filter.

Snow depth grids were calculated by differencing each snow-on DEM to the relevant snow-off DEM. The TIN-based gap-filling process of the DEMs led to a small number of artifacts that could be detected as unrealistic snow depth values in the snow depth grids. We removed these by masking out the snow depth pixels with values higher than 1.5 m and lower than −0.5 m to minimize these artifacts. The upper limit was chosen since no accumulation higher than 1.5 m was observed at our field sites. The remaining negative snow depth values (−0.5–0 m) were not removed at this stage.

Because our sites lacked permanently snow-free areas that could have served as zero snow depth reference, snow depths measured at the five stakes following each data acquisition flight were used as a final step to calibrate the snow depth raster datasets. We calculated a bulk calibration offset for each snow depth grid by averaging the difference between the in-situ snow depths measured on the snow stakes and the LiDAR-derived snow depth values at the same pixel locations.

3.3. Canopy structure data processing

The snow-off point clouds were used to create 1 m resolution canopy height models for both sites. To this end, the snow-off point clouds were first height-normalized then rasterized by the maximum normalized z-value of all the points within each 1 m pixel. The resulting canopy height model was further converted into a binary canopy map, where all pixels with canopy height $\geq$ 2 m were considered canopy pixels and all pixels with canopy height $<$ 2 m were considered non-canopy pixels. This binarization threshold is consistent with existing literature (Mazzotti et al., 2019a; Currier and Lundquist, 2018; Harpold et al., 2014) and was found to be sufficient for filtering understory vegetation. The binary canopy map provided the basis for the extraction of further canopy descriptors used in this study (see Fig. 4). We focus our analysis on canopy descriptors that characterize the local canopy structure, especially the canopy density around each pixel. The motivation for this choice is that local canopy density exerts a primary control on the

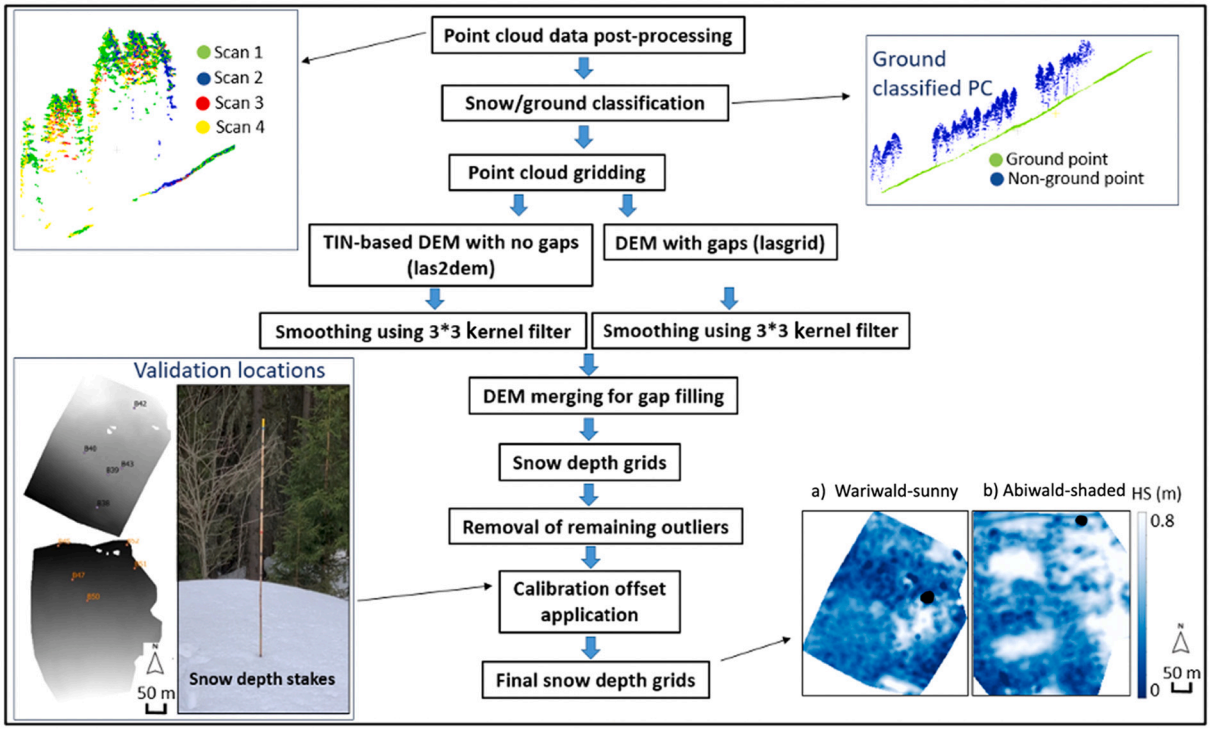

Fig. 3. Workflow to obtain snow depth maps from the raw INS data and the LiDAR returns.

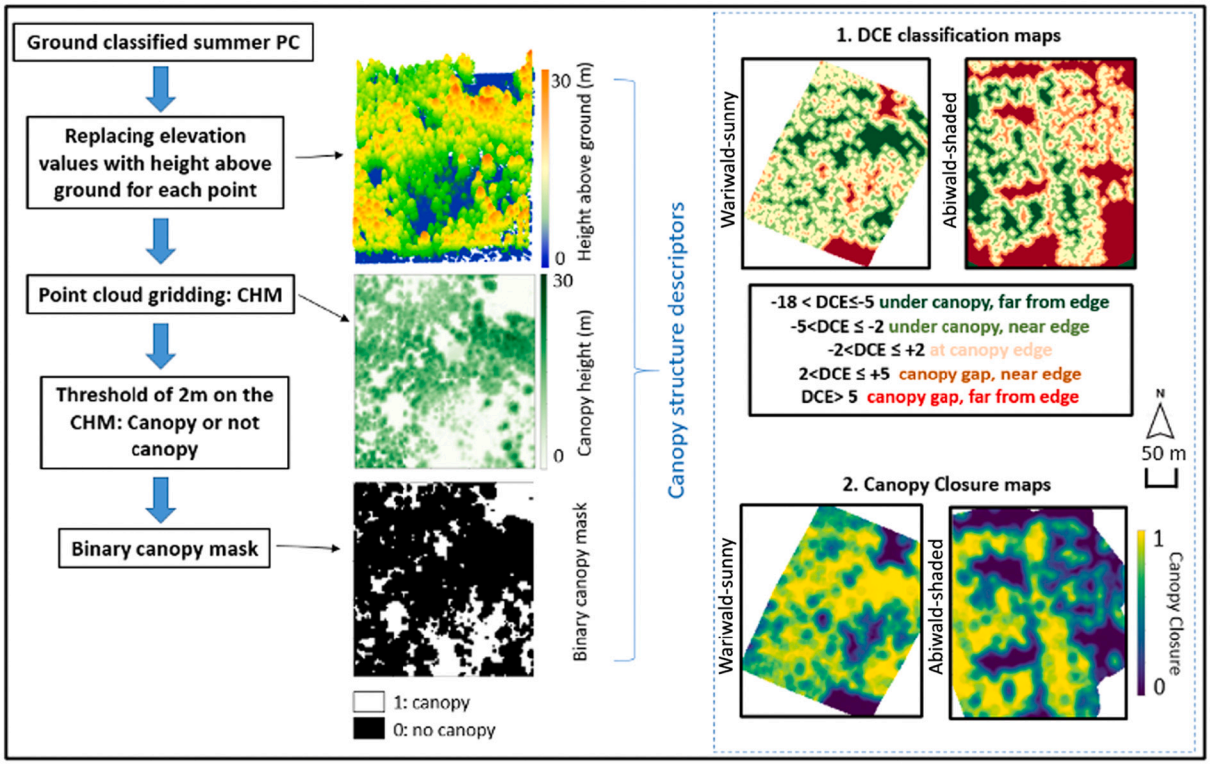

Fig. 4. Workflow illustrating the steps for the extraction of the canopy height models from the snow-off point clouds (left) as well as the two canopy structure descriptors that were estimated from the canopy height models (right).

amount of snow intercepted by the canopy, and, consequently, on snow accumulation patterns below the canopy (Broxton et al., 2015; Moeser et al., 2015; Moeser et al., 2020).

3.3.1. *Distance from canopy edge (DCE)*

The Distance to Canopy Edge (DCE, Mazzotti et al., 2019a) algorithm was used to delineate different regions within the site, representing different small-scale canopy structure categories. The DCE algorithm is an edge-detection routine, which is applied on a binary canopy map. It outputs a map at the same resolution as the binary canopy height model, where every pixel is given the value of its distance to the nearest canopy edge (DCE), with negative values denoting values inside the canopy and positive values denoting values outside the canopy, respectively (Fig. 4). The DCE maps were used to define five canopy structure classes characterizing the forest stand as follows: under canopy, far from edge; under canopy, near edge; at canopy edge; canopy gap, near edge; and canopy gap, far from edge. The corresponding DCE thresholds are reported in Fig. 4.

3.3.2. *Canopy closure (CC)*

Canopy closure (CC), defined as the percentage of canopy pixels divided by the total number of pixels around a specific pixel location within a given radius, quantifies the vertical projection of canopy cover around a point. It was derived to provide a spatially continuous quantitative measure of local canopy density at each point within the site. It is thus a second canopy descriptor, which complements the categorical DCE-based classes. In the context of this study, a radius of 5 m was chosen to compute CC (Fig. 4), since this metric was shown to have the highest spatial correlation with forest snow depth in an earlier study conducted at nearby sites with heterogeneous canopy structures (Mazzotti et al., 2020a). We chose CC as a simple and established canopy structure metric that is linked to process variability across our sites, such as the interception of snow in the canopy. It should be noted that an analogous analysis in forests with mixed species (evergreen and broadleaf) may have required the use of more sophisticated metrics (including canopy height and/or foliage density).

3.4. *Radiation modeling*

To explore the links between snow distribution and ablation processes, we further assessed sub-canopy irradiance patterns at our sites. Sub-canopy SWR and LWR are the two main drivers of snowmelt in forests, and both feature strong spatio-temporal variability (Lundquist et al., 2013; Musselman et al., 2015). The spatial distribution of sub-canopy incoming LWR is mainly dictated by sky-view fraction (V_f), which determines the patterns of LWR enhancement by the trees relative to above-canopy incoming LWR (Mazzotti et al., 2019b; Webster et al., 2017). Sub-canopy incoming LWR patterns are thus approximately constant in time. In contrast, SWR transmission is a highly complex three-dimensional process, where sub-canopy incoming SWR at any location depends on the (changing) position of the sun relative to the overhead canopy (Jonas et al., 2020; Webster et al., 2020). While V_f (and therefore incoming LWR) is itself correlated to CC (Moeser et al., 2015), incoming SWR is not. For this reason, it was of particular interest for this study to investigate the complex spatiotemporal structure of SWR input to the snow surface at our sites, in addition to CC.

SWR was assessed by applying the radiation modeling workflow described in Webster et al. (2020). This radiation model computes V_f and direct-pulse transmissivity (τ_{dir}) at each modeled location based on synthetic hemispherical images derived from LiDAR using the method from Jonas et al. (2020). Incoming SWR at a point is controlled by all canopy and terrain within a 180° hemispherical view and can be influenced by canopy up to 100 m away (Moeser et al., 2015), and terrain up to 10 km away. To include all canopy and terrain influences on measured snow depth within the field areas, the radiation model was run using ALS data collected in 2017 (Mazzotti et al., 2019a). A visual comparison between the 2017 data and the point clouds collected in this study showed no changes in canopy structure between the two data

acquisitions. The model included both canopy and terrain effects on SWR transmission.

Total sub-canopy incoming SWR is given by the sum of above-canopy direct and diffuse SWR components multiplied by τ_{dir} and V_f, respectively. We used the open-site SWR data recorded at the Davos meteorological station (section 2.3) as a proxy for the above-canopy SWR. To partition the total above-canopy incoming solar radiation into diffuse and direct components, we used the scheme presented in Erbs et al. (1982), which estimates this partitioning based on atmospheric transmissivity. The calculation of the atmospheric transmissivity requires the solar zenith angle, which we computed with the parameterization developed by NOAA (https://www.esrl.noaa.gov/gmd/grad/solcalc/calcdetails.html).

Total sub-canopy SWR was calculated at every pixel and for hourly timesteps between December 1st 2019 and the end of our observation period. Additionally, the cumulative SWR input between the beginning of December and each flight date was computed. The workflow is shown in Fig. 5, yielding cumulative sub-canopy SWR input maps at 1 m resolution for both sites and each data acquisition date. Note that our approach only allowed to infer the spatio-temporal variability of incoming radiation components, contrary to studies such as Malle et al. (2019) and Hotovy and Jenicek (2020) who were able to quantify net radiative fluxes owing to the measurement of the upwelling radiation components. Such data were unavailable at our site; analysis of spatio-temporal variation in net snowpack energy fluxes was thus beyond the scope of this study.

4. Results

4.1. Snow depth maps accuracies

Manually measured and LiDAR-derived snow depths were compared and the coefficients of determination (R^2) were calculated for both sites separately, before and after the implementation of the calibration offset (Fig. 6a and b). Based on these graphs, a systematic bias can be excluded and mismatches between the manual measurements and the LiDAR data mainly attributed to noise. The match between the manual measurements and the LiDAR data was quantified in terms of root mean squared error (RMSE) for all the dates. The RMSE fluctuates between 5 and 17 cm and 5–10 cm for Wariwald-sunny and 5–21 cm and 4–20 cm for Abiwald-shaded before and after applying the calibration offset (Fig. 6c). The average RMSEs for all the dates presented in Fig. 6c is 13 cm and 11 cm for Abiwald-shaded and 11 cm and 8 cm for Wariwald-sunny (before/after the calibration offset). The comparison of the RMSE values for both sites reveals that in Wariwald-sunny the accuracies are higher than in Abiwald-shaded. This is in accordance to the expected increased vertical biases of a LiDAR system in steeper terrain since Abiwald-shaded is steeper than Wariwald-sunny on average. Note that data acquired at Abiwald-shaded on the 3rd and 27th of April had to be discarded from our analysis due to an unacceptable level of noise despite following the workflow outlined in section 3.1.

4.2. Spatio-temporal snow distribution dynamics relative to canopy structure

This section relates snow distribution patterns to canopy structure at the two sites. In the first sub-section, snow depth distribution is qualitatively compared to the canopy height models. In the second sub-section, a more quantitative exploration of snow depth evolution in the context of the DCE-based canopy classes is presented.

4.2.1. Qualitative overview of snow depth pattern evolution

Fig. 7 presents the snow depth patterns at the two sites for three representative dates corresponding to roughly the beginning (7th February) and the end of the accumulation phase (i.e. peak of winter, 11th March), and the middle of the ablation phase (1st of April). The canopy height models of the two sites are displayed for reference. Overall, these data reveal that the highest snow depths were consistently found in forest gaps, while snow amounts in the below- and close-to-canopy areas were generally lower. The snow depths reached their highest values on the 11th of March for both sites throughout the forest.

However, comparing the two sites also highlights some important differences: The gaps in Abiwald-shaded featured deeper snow depths during the three depicted dates than the gaps in Wariwald-sunny. The gaps in Abiwald-shaded retained snow depths up to 80 cm even at the beginning of April whereas the snow depths were close to zero under dense canopy. In contrast, gaps at Wariwald-sunny had less snow throughout the season and retained less snow at the beginning of April

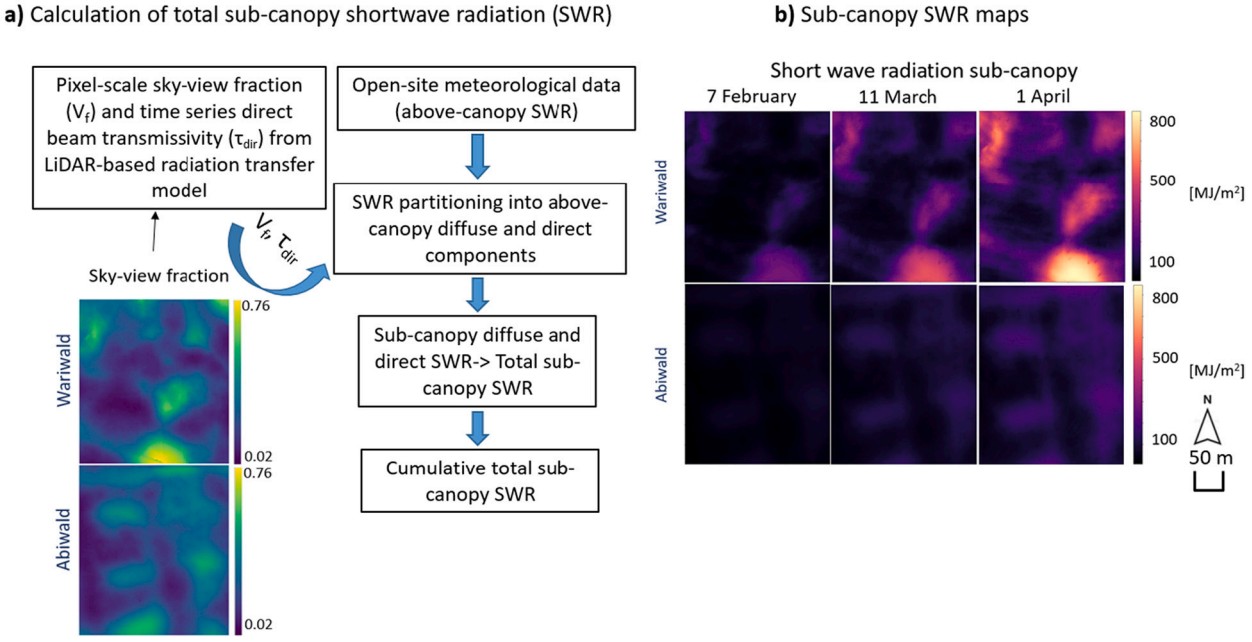

Fig. 5. (a) Workflow for the calculation of the incoming sub-canopy cumulative SWR that reaches the snow surface from the 1st of December until each flying date; (b) SWR maps for three representative dates.

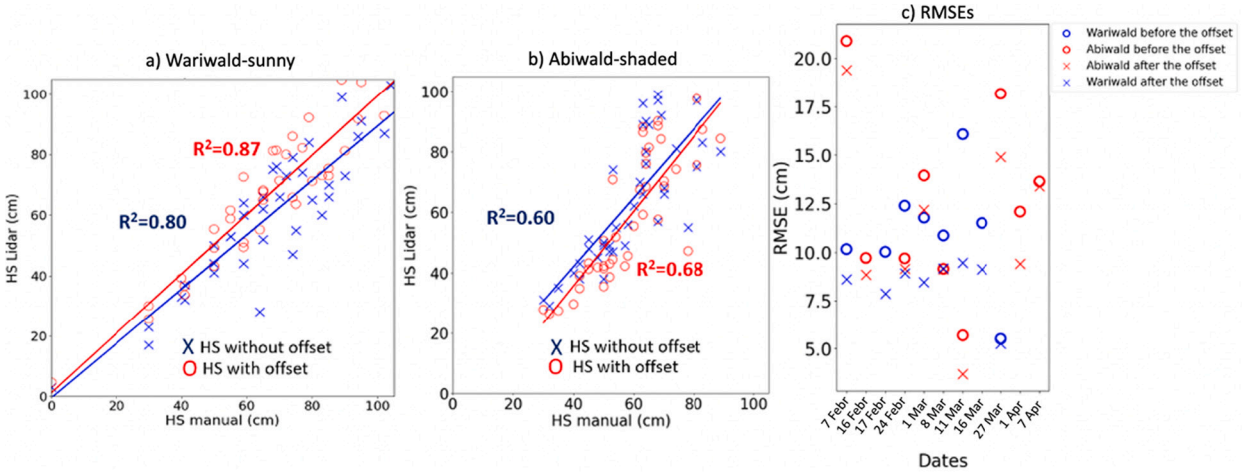

Fig. 6. Scatterplots of manual against LiDAR-derived snow depths for Wariwald-sunny (a) and Abiwald-shaded (b); RMSE for all the dates and both sites, after applying the calibration offset on each snow depth grid (c).

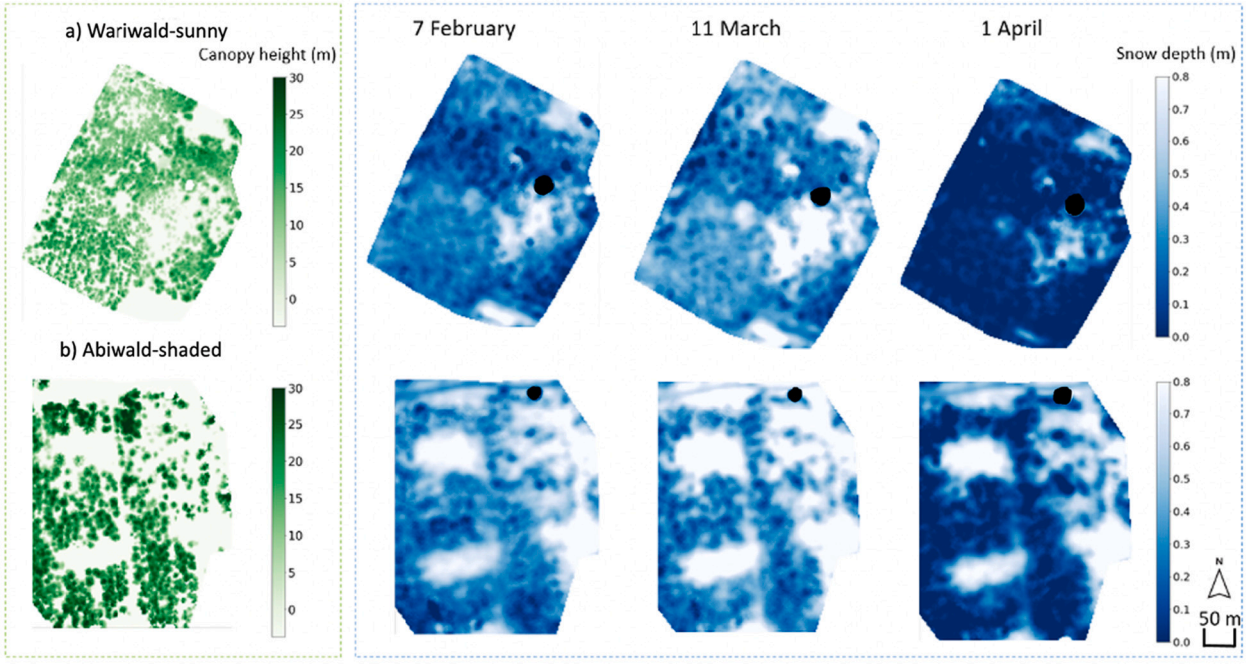

Fig. 7. Snow maps for the two sites for three representative dates (right) where black shading denotes no data, and the respective canopy height models (left).

compared to Abiwald-shaded. The snow patterns for the three dates also show that Wariwald-sunny became snow-free earlier than Abiwald-shaded, especially in the areas below canopies which were already almost snow-free at the beginning of April. Notably, the gap on the lower-south part of the forest was almost snow-free by that time as well.

4.2.2. Snow depth evolution for the DCE-based classes

For a more quantitative assessment of snow depth dynamics relative to canopy structure, the evolution of the mean snow depth per DCE-based class for both sites is presented in Fig. 8. These plots confirm the general increase in snow depth from dense canopies towards large gaps identified in section 4.2.1. Comparing both sites, there was more snow at Abiwald-shaded than at Wariwald-sunny for DCE each class and acquisition, and the differences between the two sites increased throughout the ablation period. In the canopy gaps (see corresponding DCE classes), snow depths did not exceed 70 cm at Wariwald-sunny, with the highest average of the respective classes found on the 11th of March (peak of winter). On the same date, the corresponding mean snow depth value reached almost 1 m in the gaps at Abiwald-shaded. During all the dates, the mean snow depths at Wariwald-sunny remained between 20 and 60 cm in the gaps, whereas for all the corresponding dates at Abiwald-shaded the snow depths in the gaps had higher values, between 20 and 80 cm.

We further observed a different temporal evolution of the mean snow depth per class at the two sites: In Abiwald-shaded the mean snow depth increased steadily from the two under-canopy classes to the gaps away from the canopy edges, and this behavior was consistent throughout the season. Wariwald-sunny showed the same behavior, but in this case, there was no discernible difference in the mean snow depths between the two DCE classes below-canopy and in the gaps. Furthermore, the data at Wariwald-sunny suggest a faster snow depletion rate in gaps than below canopy right after the peak of snow. As the first acquisitions after

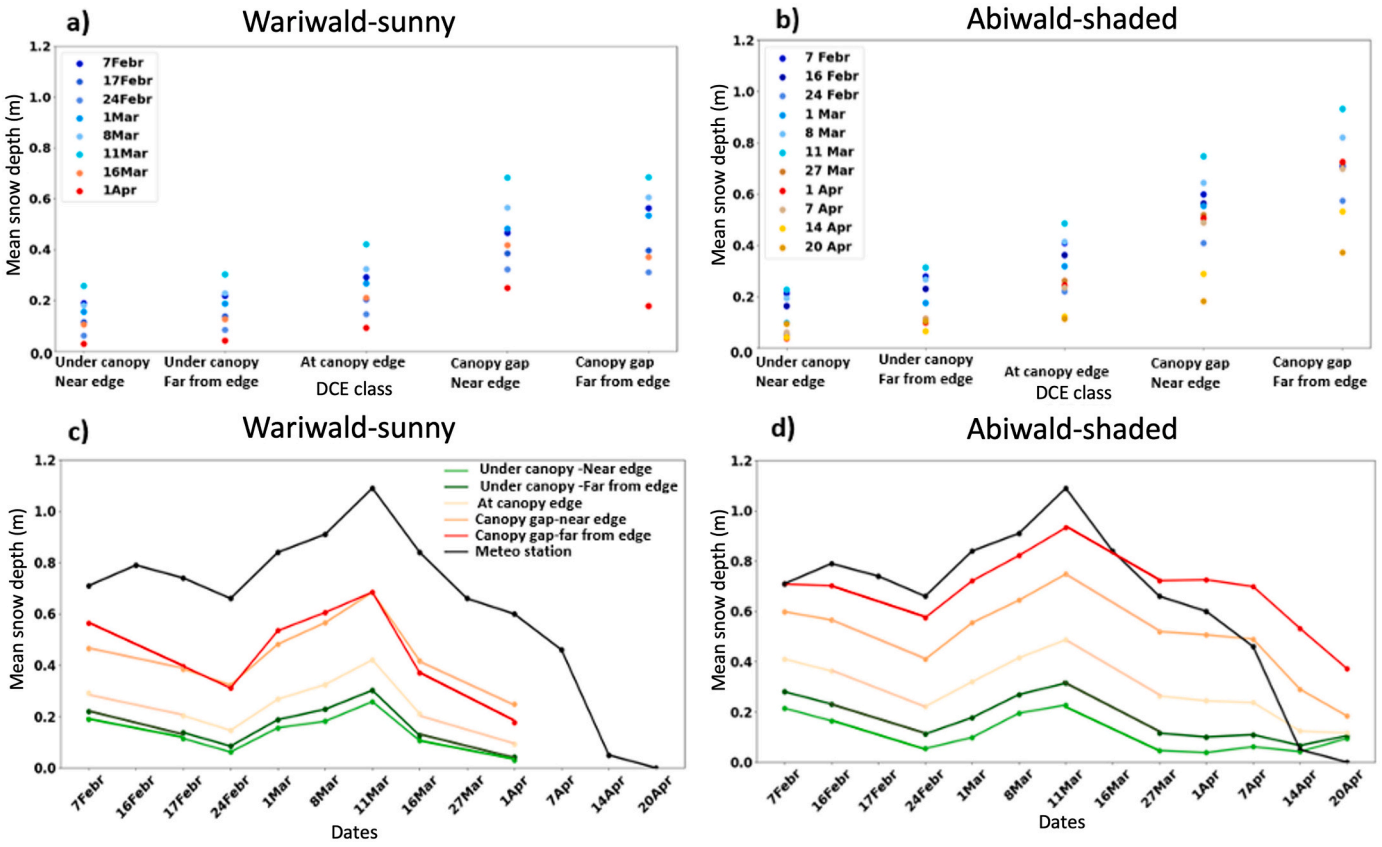

Fig. 8. Overview of snow depths per DCE class at the two slopes over the entire season (a and b) and mean snow depths per DCE class for all the dates and both sites (c and d).

peak snow still featured 100% snow coverage, this finding indicates that the slower depletion in areas with, on average, less snow, was not only an effect of partial snow cover.

Mean snow depths for each class at both sites are further compared to the snow depths measured at the reference open site (Fig. 8; black lines in lower panels). In Wariwald-sunny, the snow accumulation in the open site was almost 20 cm higher than in the gaps. On the contrary, in Abiwald-shaded there was almost the same amount of snow in the gaps compared to the open site during accumulation. After the onset of snowmelt (11th of March onwards), this trend shifted and the canopy gaps at Abiwald-shaded retained, on average, greater snow depths than the open site. Consequently, melt-out at the open site (April 20th) occurred earlier than for any DCE class in Abiwald-shaded, but later than in Wariwald-sunny, which was largely snow-free by that time.

4.3. Spatio-temporal dynamics of sub-canopy incoming SWR

To provide context to the between-sites differences identified by the results presented in section 4.2, this section provides an analysis of sub-canopy incoming SWR dynamics relative to canopy structure at the two sites. Fig. 9 presents the evolution of cumulative sub-canopy incoming SWR for both sites. Fig. 9a shows the site-averaged sub-canopy incoming SWR for all flight dates throughout the whole data acquisition period. The cumulative average sub-canopy SWR input increased steadily over time at both sites, but it is larger for Wariwald-sunny than for Abiwald-shaded for all the dates. While this finding was expected due to the orientation of the two sites, it is worth noting since the average CC at Abiwald-shaded was lower (0.55) than Wariwald-sunny (0.71).

Within-site differences in cumulative incoming sub-canopy SWR are visualized in Fig. 9b, expressed as average sub-canopy incoming SWR within each DCE-based class for three representative dates (see Fig. 7). All the five different classes at Wariwald-sunny received more SWR than the corresponding classes at Abiwald-shaded, for all three dates. For reference, the class-average of cumulative sub-canopy incoming SWR in the largest gaps at Abiwald-shaded on April 1st was of comparable magnitude to cumulative sub-canopy incoming SWR under the dense canopy at Wariwald-sunny for the same date. At the same time, it was still lower than cumulative sub-canopy incoming SWR for the same canopy class at Wariwald-sunny on February 7th.

Both differences between classes for the same site and between sites for the same class increased over the season, mainly due to increasing cumulative above-canopy incoming SWR. However, due to its exposure to direct insolation, Wariwald-sunny featured a stronger increase in sub-canopy incoming SWR over time than Abiwald-shaded, which resulted in larger between-class differences. At Abiwald-shaded, in contrast, given the lack of direct insolation, the differences between classes only reflected spatial variation in sub-canopy diffuse SWR, which is controlled by V_f. Overall, this analysis illustrates how the controls of terrain (i.e. exposure) on incoming solar radiation to the snow surface can be of similar or larger magnitude as controls exerted by the canopy.

4.4. Correlations between snow distribution and local canopy structure

We finally combine findings from sections 4.2 and 4.3 to explain correlation patterns between snow depth distribution and local canopy structure, and how they varied in time between the two sites. Fig. 10a shows the temporal evolution of the correlations between local CC and snow depths, which is further illustrated by the density scatterplots of CC versus snow depth for the three representative dates at both sites (Fig. 10c). The evolution of the correlation coefficients is further compared to the evolution of mean snow depth at each site throughout the season (Fig. 10b). Two key observations follow from these graphs.

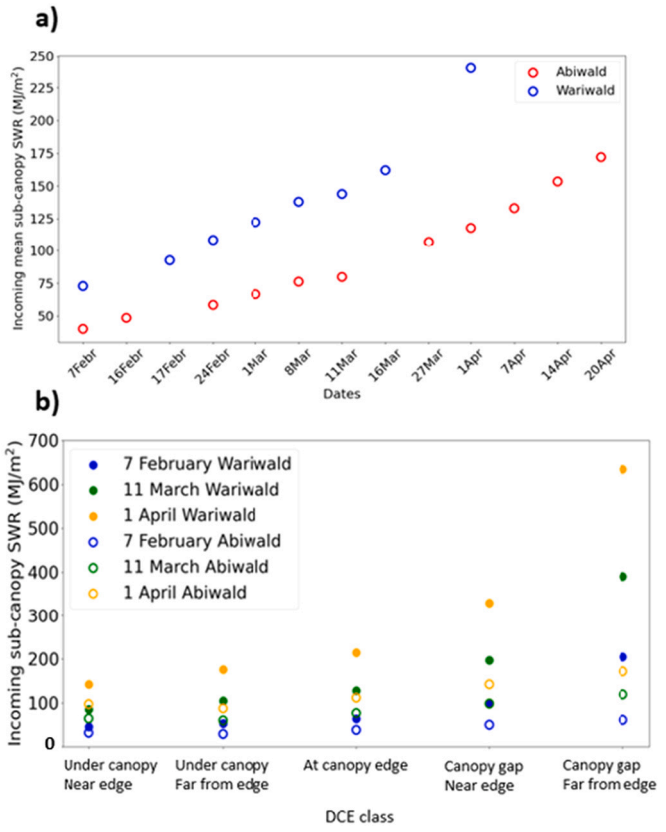

Fig. 9. Mean cumulative sub-canopy incoming SWR starting from the 1st of December (a) for all the dates and (b) per DCE class for three representative dates for both sites.

Firstly, the negative correlation between local CC and snow depth was consistently stronger for Abiwald-shaded than for Wariwald-sunny: In fact, the Pearson correlation coefficient at Abiwald-shaded reached values around −0.8 for a large part of the season (around −0.85 on the 11th March which was the date with the strongest correlation), while the strongest correlation coefficients varied between −0.6 and − 0.7 at Wariwald-sunny. Secondly, this correlation persisted for a longer time at Abiwald-shaded than at Wariwald-sunny. At Abiwald-shaded, correlations were still strong for part of the ablation season and only weakened for the two last campaigns as snow cover started to become partial. In contrast, the correlation strength deteriorated right at the peak of winter at Wariwald-sunny ($R = -0.5$ on March 16).

The vertically projected local canopy cover, here quantified by way of CC, is influential to processes driving sub-canopy snow accumulation and depletion dynamics, such as interception/throughfall and LWR. SWR represents an important exception: As a three-dimensional process, its complex spatiotemporal dynamics did not exhibit a direct dependence on a local and purely two-dimensional canopy descriptor. Based on our analyses, we can thus suggest an interpretation of the difference in snow distribution dynamics between the two sites in terms of the varying relative importance of different physical processes at the two sites.

Snow depth distribution early in the snow season was majorly affected by accumulation processes. At our sites, interception patterns were the main driver of snow cover dynamics during this phase, supported by the strongest correlations of snow depth and CC generally occurring during accumulation at both sites. The weaker correlations observed for Wariwald-sunny compared to Abiwald-shaded, however, were likely caused by the different exposure to direct SWR experienced by the two sites. Wariwald-sunny received much more sun already during the accumulation period (see Fig. 9), resulting in superimposed interception and insolation patterns at Wariwald-sunny but not at Abiwald-shaded. Additionally, stronger insolation also leads to more settling and/or midwinter melt, which also explains the lower average snow depths at Wariwald-sunny compared to Abiwald-shaded observed

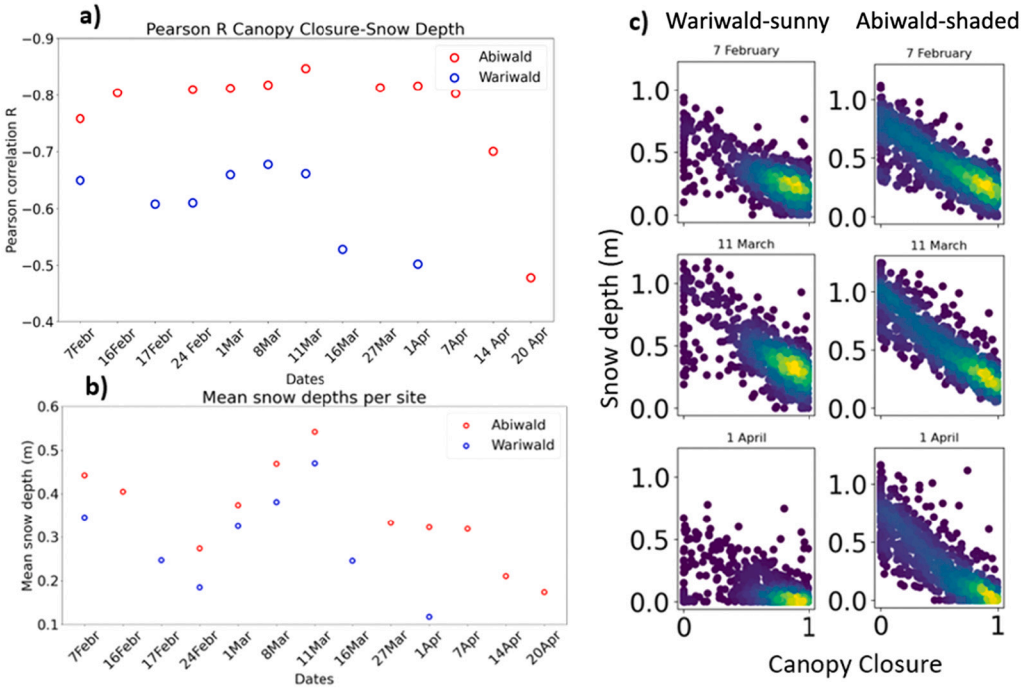

Fig. 10. Pearson Correlation coefficient between CC and snow depth in time for both sites (a); Evolution of the mean snow depths per site and for all the dates (b); Density scatterplots between CC and snow depth for three representative dates for both sites (c).

already during accumulation.

After the peak of winter, ablation processes can either exacerbate or diminish the initial correlation between snow distribution and local CC, depending on whether or not the ablation patterns themselves are spatially correlated with CC. No precipitation event occurred after March 11th. At Wariwald-sunny the process of insolation that already superimposed the accumulation processes immediately became the dominant control on snow distribution. At Abiwald-shaded, SWR input was likely too weak to disrupt the patterns created by accumulation processes, shown by the continually strong correlations between snow depth and CC into the ablation period. Due to the lack of direct insolation, LWR was likely the main driver of snow ablation at this site.

Overall, these findings reveal a higher complexity of the snow distribution dynamics and its relationship to canopy structure characteristics at Wariwald-sunny. As shown by our analysis, this is linked to the longer and stronger exposure to the sun at this south-exposed side, as this entails the concurrent influence of processes that feature dissimilar canopy structure dependencies throughout the season.

5. Discussion

5.1. The interplay between canopy structure and topography shapes snow distribution dynamics in forested slopes

The dataset presented in this study allowed a detailed comparison of forest snow dynamics and their spatio-temporal evolution at two opposing slopes using a UAV-borne LiDAR system. Snow cover dynamics were not only linked to a static canopy structure descriptor as in earlier studies (Broxton et al., 2015; Hojatimalekshah et al., 2021; Moeser et al., 2020), but also to detailed sub-canopy SWR. The SWR dynamics at the two slopes exhibited substantial differences due to different topographic shading. Hence, our analysis enabled interesting insights into how topography and canopy structure interact to alter the relative importance of processes shaping snow cover dynamics at opposed slopes. These interactions, in turn, were shown to create distinctly different snow distribution pattern evolution at the two slopes.

The general snow depth decrease from gaps to the dense canopy, which was shown using DCE-based classes, confirming findings of previous studies of Broxton et al. (2015), Mazzotti et al. (2019a), Moeser et al. (2015). However, our data also revealed generally higher mean snow depths in the shaded slope (Abiwald) compared to the sunny slope (Wariwald) throughout the season, particularly in the gaps. The close vicinity of the two sites means that any considerable differences in precipitation input and wind can be excluded, meaning accumulation processes at both sites adhere to the meteorological patterns. With SWR being the only highly variable meteorological input between sites, it is likely that SWR is the main driver of the differences in snow distribution patterns between the two sites. These findings support earlier observations by Golding and Swanson (1986) and Ellis et al. (2011), who established that the snow accumulation in forest clearings is affected by the exposure to solar radiation. Smaller mean snow depths in dense canopy areas than in open areas and accelerated melt at south-exposed forested slopes were also reported by Cartwright et al. (2020). Broxton et al. (2020), focusing on water equivalent estimations found accumulation around 20–30% higher in gaps than in under-canopy areas and ablation rates at south-exposed slopes increased up to 15–30% relative to the north-exposed slopes. Zheng et al. (2016) found canopy strcuture and topographic characteristics to be relevant explanatory variables of snow distribution, using LiDAR-derived snow depths and regression analysis over a site in the Sierra Nevada. Very recently, the combined impact of canopy structure and topography was evidenced in a study by Safa et al. (2021), who applied machine learning algorithms to several LiDAR-derived snow distribution datasets from the Western US.

Between-site differences throughout the season, illustrated by the different evolutions of the correlations between snow depth and CC at the two sites, demonstrate that discrepancies in snow cover dynamics between slopes of different aspects already build up during the accumulation and not only during the ablation period. This is in line with the study of Grünewald et al. (2010), conducted in open terrain, which showed that areas of different aspects were characterized by different accumulation rates and also had differential depletion over the entire season. Schirmer and Pomeroy (2020) also highlighted that solar irradiance input in areas with different aspects causes different ablation rates and differences in early-season melting. Kostadinov et al. (2019) found higher fractional snow cover for below-canopy areas compared to open areas on south-exposed slopes at high elevation, confirming the dominant role of radiative processes in shaping snow distribution patterns during ablation.

Our results have important implications in the context of forest snow modeling. Latest hyper-resolution models that account for small-scale canopy structure and its influence on accumulation processes and radiation patterns (Broxton et al., 2015; Moeser et al., 2020) should be inherently capable of resolving differences in snow cover dynamics between slopes. However, most models operate at coarser resolution and need to capture variability induced by canopy structure at the sub-grid level, either by parametrizations (Luce and Tarboton, 2004) or sub-tiling schemes (Currier and Lundquist, 2018). As suggested e.g. by Dickerson-Lange et al. (2015) and Mazzotti et al. (2021), sub-grid parametrizations specifically tailored to forested areas should be a priority of future research in the field. Our findings, indicate that such parametrizations would need to incorporate both, canopy structure and topography information, due to the distinct snow distribution patterns created by the two. Forest snow distribution maps as presented in this study could provide the basis for the sub-grid parametrizations, however, it should be kept in mind that the TIN-based gap filling method applied here likely overestimates snow depth under canopies and should be revisited in the context of LiDAR-derived forest snow maps.

While providing meaningful insights, our analysis disregarded some factors that may additionally impact snow distribution patterns. Firstly, it should be pointed out that our findings are specific to the meteorological characteristics typical of our alpine sites. For instance, accumulation patterns were unaffected by wind, due to generally low wind speeds given the location of our sites within larger forest stands (Mazzotti et al., 2020b), as well as relatively warm temperatures during snowfall events leading to limited wind transport (Mott et al., 2018). Studies conducted in colder and windier climates of the Western United States (Currier and Lundquist, 2018; Webb et al., 2020) have reported substantial snow redistribution by wind, which created accumulation patterns that were not directly linked to CC. Also, the ablation season in our study was characterized by fine weather and long periods of clear sky conditions. Under these conditions, direct solar radiation prevails, maximizing differences due to topography, and the range of LWR enhancement is largest, maximizing the link between LWR-driven ablation and CC (Mazzotti et al., 2019b). Prevalence of cloudy conditions would have shifted the radiation patterns to more homogeneous LWR enhancement and stronger impact of diffuse radiation (i.e. negative correlation to CC). Such meteorological conditions would therefore likely have led to a faster decay of the correlation between snow depth and CC at Abiwald-shaded during the ablation season, and smaller differences between the two sites. Consequently, and as suggested in existing literature (e.g. Mazzotti et al., 2021), any upcoming sub-grid forest snow parametrization should account for different controls relevant in different climates, and only be applied in the context of the climatic conditions for which it has been developed.

Secondly, and also as pointed out in previous literature, microtopography (Hopkinson et al., 2012; Cho et al., 2021), as well as the ground roughness (Lehning et al., 2011; Cho et al., 2021), are additional controls on snow distribution that may confound canopy structure and topography effects. The forest floor at our sites indeed featured a considerable degree of roughness, due to rocks, fallen logs, and shrubs. However, initial attempts to characterize ground roughness from the snow-off LiDAR point cloud were unsuccessful, which hampered us from

investigating its influence on snow cover dynamics. Finally, our data was only able to capture snow depth distribution and could not resolve spatial differences in snow density, which does exhibit considerable variability in forests (Broxton et al., 2020; Raleigh and Small, 2017). While still providing insightful findings of the relative importance of different processes, our study cannot offer a full assessment of canopy and topographic impacts on snow water resources in terms of snow water equivalent. Canopy-class-specific snow density surveys at the two slopes would have been a useful complement to our dataset for this purpose. Unfortunately, accessibility restrictions made such efforts unfeasible.

5.2. Technical challenges, lessons learned, and recommendations for future UAV-borne LiDAR forest snow studies in steep slopes

The flexibility and the cost-effectiveness of UAVs make them an attractive tool for snow distribution surveying at high spatio-temporal resolutions. Given the unique assets of UAV-borne LiDAR compared to other platforms (e.g. LiDAR from crewed aircraft or UAV-borne optical sensors), it is a suitable choice for snow mapping studies on forested slopes. While a thorough accuracy assessment of this technology was beyond the scope of this study, the comparison against ground truth data (section 4.1) suggests that measurement errors were in the same order of magnitude as those observed for ALS-based studies in flat forests (Currier et al., 2019; Mazzotti et al., 2019a; Harder et al., 2020; Jacobs et al., 2021). However, our experience revealed that UAV-borne LiDAR technology is not straightforwardly applicable and that it comes with many challenges related both to the field data acquisition and the subsequent data processing. Specific challenges we faced are discussed below followed by recommendations for future applications of this promising technology.

The LiDAR-integrated INS proved to have operational difficulties, which became evident when analyzing misalignments between strips that persisted even after the PPK corrections. This could have been due to a changing flying height along the individual flight lines, which was implemented to maintain a fixed height above the terrain. Since no such difficulties were encountered with the same system when maintaining a constant flying height above flat terrain (see Koutantou et al., 2021), we conclude that higher-grade INS may be beneficial for such terrain-following applications for surveying in steep terrain.

The return density of 30 pts./m^2 granted by our LiDAR system is sufficient for resolving forest snow patterns at the meter scale and was comparable to other studies investigating snow depth distribution with ALS data (e.g. 18 pt./m^2 in Currier et al. (2019), 5–30 pt./m^2 in Mazzotti et al. (2019a) and 10–15 pt./m^2 in Broxton et al. (2020)). However, occlusion turned out to be a limiting factor. Despite the manufacture-stated ability to record up to three returns per pulse, an inspection of our datasets revealed that most pulses yielded one return only, which meant that oftentimes the LiDAR pulse did not manage to penetrate the canopy. The overlapping flight patterns that yielded point densities of around 120 pts./m^2 were designed to compensate for this circumstance and allowed us to restrict data gaps below the canopy to an acceptable level. However, this required strategy substantially reduced the area we could cover with our set of batteries. The resulting trade-off between spatial extent covered and point density achieved may have been avoided with a different LiDAR system, e.g. a system able to output the full waveform data to allow identifying even weak returns, e.g. such as the system used by Harder et al. (2020). Considering the amount of data gaps below dense canopy areas we still faced despite the high point densities reached by overlapping flight plans, we strongly advocate a careful choice of LiDAR system and survey parameters for forest snow studies, as these have different data requirements than typical applications of LiDAR. High pulse frequency, small pulse divergence and multi-angular scanning, as well as the possibility to post-process full waveform data would improve the concurrent capture of both canopy and the below-canopy surface. Where data gaps cannot be avoided, more sophisticated gap filling algorithms could be explored to avoid the likely overestimation of snow depth caused by the TIN-based gap-filling method used here. While already suggested by Mazzotti et al. (2019), the enhancement of this algorithm was beyond the scope of this study as it would require substantially more ground validation measurements.

The manual registration adjustment procedure we had to apply to compensate for a lack of positioning accuracy of the INS is not considered part of a standard processing workflow. In fact, such a step is not reported by either Jacobs et al. (2021), Harder et al. (2020) or Cho et al. (2021). Yet, it was indispensable in our case, as misalignment issues and data gaps not only affected the accuracy of our data but substantially inhibited the application of subsequent processing algorithms. As discussed in detail in Koutantou et al. (2021) numerous existing algorithms were unsuccessfully tested prior to adopting the manual registration workflow. A major limitation to the use of these algorithms was the lack of stable objects at our sites that could have been used as tie points in feature-based registration algorithms. Since our acquisitions only occurred in the absence of wind and snow intercepted in the canopies, we even tested the use of treetops as stable features within our sites, as proposed by Ferraz et al. (2018), but failed to extract a global rotation and translation matrix applicable to the whole point cloud.

A large set of Ground Control Points (GCPs) would have facilitated the registration procedures. We strongly recommend that future forest snow studies involve permanently installed GCPs that are evenly distributed across the site, to allow minimizing geolocation errors homogeneously across the entire point cloud. Snow depth measurements on the GCPs could be also useful for the validation of the snow depth maps. As with the GCPs, an even distribution of the validation stakes across the sites is recommended (Bühler et al., 2015, 2016; Vander Jagt et al., 2015; Avanzi et al., 2018). This was not possible at our sites due to accessibility issues; disturbance of the snow surface needed to be minimized, and especially at Abiwald-shaded, accessibility was only granted at the lower end of the slope for avalanche safety reasons. An alternative solution could be the placement of stakes with cameras oriented towards them to avoid necessitating direct access to them on each campaign day. Where snow-free areas are present, a combination of the LiDAR datasets with optical imagery could be used to delineate these for later use to facilitate the registration of snow-on and snow-off point clouds, as in the workflow applied by the Airborne Snow Observatory (Painter et al., 2016). Snow-free features could also provide a more robust validation target than point measurements from snow stakes.

6. Conclusions

This study presented, for the first time, an analysis of spatio-temporal snow dynamics in two heterogeneous forests on slopes of opposing aspects, based on repeated UAV-borne LiDAR surveys. Snow depth maps at 1 m resolution derived from the point clouds were analyzed in conjunction with canopy structure information and detailed maps of sub-canopy incoming shortwave radiation obtained with a LiDAR-based radiation transfer model.

Analysis of co-registered snow and canopy structure data revealed a strong correlation between spatial patterns of snow depth and local canopy closure early in the season. This correlation was stronger and persisted longer for the north-exposed site, but was weaker and decayed immediately after the peak of winter at the south-exposed site. The temporal evolution of the correlation between snow depth and local canopy closure suggests that at the shaded slope, snow distribution patterns were mainly governed by interception patterns formed during accumulation, and were not significantly altered during ablation. These consistent snow depth distribution patterns through the ablation period suggest longwave radiation was the dominant radiation flux at the shaded site. In contrast, direct insolation was the dominant radiation flux at the south-exposed slope, and its complex spatio-temporal patterns lead to snow distribution dynamics that exhibit a less well-defined link to the local structure throughout the ablation period.

These findings corroborate the complexity of the snow processes in forests and the important role both local canopy cover and topography play in shaping them. Approaches to parametrize the sub-grid variability of forest snow in coarse-resolution models will thus need to account for both, and such approaches must be tested in a variety of topographic settings and meteorological conditions.

In general, the UAV-borne LiDAR system proved efficient in mapping snow cover dynamics with a high spatial and temporal resolution. However, we identified technical challenges specific to applying this technology to forested slopes. Future application of UAV-borne LiDAR to snow studies in forested complex terrain should carefully consider system specifications and the use of GCPs to facilitate subsequent data processing. Concurrent acquisition of snow density measurements would further allow extending this snow depth-based analysis to snow water equivalent in view of a more accurate quantification of snow water resources.

CRediT authorship contribution statement

Kalliopi Koutantou: Methodology, Data curation, Formal analysis, Software, Investigation, Visualization, Writing – original draft. **Giulia Mazzotti:** Conceptualization, Methodology, Investigation, Validation, Writing – review & editing. **Philip Brunner:** Project administration, Funding acquisition, Supervision, Writing – review & editing. **Clare Webster:** Software, Writing – review & editing. **Tobias Jonas:** Conceptualization, Supervision, Resources, Writing – review & editing.

Declaration of Competing Interest

The authors declare that they have no known competing financial interests or personal relationships that could have appeared to influence the work reported in this paper.

Acknowledgments

The UAV and LiDAR systems were funded by the Swiss National Science Foundation (SNSF, R'Equip grant 206021_170753). Kalliopi Koutantou and Philip Brunner were supported by the University of Neuchatel, Giulia Mazzotti, Clare Webster and Tobias Jonas by WSL/SLF. The authors would like to thank the Snow Hydrology team from SLF for their assistance in the field whenever needed, as well as the members of the electronics team from SLF that were assisting with the UAV technical issues. The acquisition of LiDAR and validation data would not have been possible without the help of Laurent Fasnacht and Eliane Brändle, for assisting with the UAV flight plans and for being the main copilot during the UAV flights, respectively. Finally, the authors would like to thank two anonymous reviewers and the editors for their constructive comments.

References

Applanix, 2019. POSPac UAV, Version 8.3, Licensed.

Avanzi, F., Bianchi, A., Cina, A., De Michele, C., Maschio, P., Pagliari, D., Passoni, D., Pinto, L., Piras, M., Rossi, L., 2018. Centimetric accuracy in snow depth using unmanned aerial system photogrammetry and a multistation. Remote Sens. 10 (5), 765. https://doi.org/10.3390/rs10050765.

Bebi, P., Seidl, R., Motta, R., Fuhr, M., Firm, D., Krumm, F., Conedera, M., Ginzler, C., Wohlgemuth, T., Kulakowski, D., 2017. Changes of forest cover and disturbance regimes in the mountain forests of the Alps. For. Ecol. Manag. 388, 43–56. https://doi.org/10.1016/j.foreco.2016.10.028.

Björk, R.G., Molau, U., 2007. Ecology of alpine snowbeds and the impact of global change. Arct. Antarct. Alp. Res. 39 (1), 34–43. https://doi.org/10.1657/1523-0430(2007)39[34:EOASAT]2.0.CO;2.

Broxton, P.D., Harpold, A.A., Biederman, J.A., Troch, P.A., Molotch, N.P., Brooks, P.D., 2015. Quantifying the effects of vegetation structure on snow accumulation and ablation in mixed-conifer forests. Ecohydrology 8 (6), 1073–1094. https://doi.org/10.1002/eco.1565.

Broxton, P.D., Leeuwen, W.J.D., Biederman, J.A., 2020. Forest cover and topography regulate the thin, ephemeral snowpacks of the semiarid Southwest United States. Ecohydrology 13 (4). https://doi.org/10.1002/eco.2202.

Bründl, M., Etter, H.-J., Steiniger, M., Klingler, Ch., Rhyner, J., Ammann, W.J., 2004. IFKIS - a basis for managing avalanche risk in settlements and on roads in Switzerland. Nat. Hazards Earth Syst. Sci. 4 (2), 257–262. https://doi.org/10.5194/nhess-4-257-2004.

Bühler, Y., Marty, M., Egli, L., Veitinger, J., Jonas, T., Thee, P., Ginzler, C., 2015. Snow depth mapping in high-alpine catchments using digital photogrammetry. Cryosphere 9 (1), 229–243. https://doi.org/10.5194/tc-9-229-2015.

Bühler, Y., Adams, M.S., Bösch, R., Stoffel, A., 2016. Mapping snow depth in alpine terrain with unmanned aerial systems (UASs): potential and limitations. Cryosphere 10 (3), 1075–1088. https://doi.org/10.5194/tc-10-1075-2016.

Cartwright, K., Hopkinson, C., Kienzle, S., Rood, S.B., 2020. Evaluation of temporal consistency of snow depth drivers of a Rocky Mountain watershed in southern Alberta. Hydrological Processes. 34, 4996–5012. https://doi.org/10.1002/hyp.13920.

Cho, E., Hunsaker, A.G., Jacobs, J.M., Palace, M., Sullivan, F.B., Burakowski, E.A., 2021. Maximum entropy modeling to identify physical drivers of shallow snowpack heterogeneity using unpiloted aerial system (UAS) lidar. J. Hydrol. 602, 126722 https://doi.org/10.1016/j.jhydrol.2021.126722.

Clark, M.P., Hendrikx, J., Slater, A.G., Kavetski, D., Anderson, B., Cullen, N.J., Kerr, T., Örn Hreinsson, E., Woods, R.A., 2011. Representing spatial variability of snow water equivalent in hydrologic and land-surface models: a review: representing spatial variability of swe in models. Water Resour. Res. 47 (7) https://doi.org/10.1029/2011WR010745.

Currier, W.R., Lundquist, J.D., 2018. Snow depth variability at the forest edge in multiple climates in the Western United States. Water Resour. Res. 54 (11), 8756–8773. https://doi.org/10.1029/2018WR022553.

Currier, W.R., Pflug, J., Mazzotti, G., Jonas, T., Deems, J.S., Bormann, K.J., Painter, T.H., Hiemstra, C.A., Gelvin, A., Uhlmann, Z., Spaete, L., Glenn, N.F., Lundquist, J.D., 2019. Comparing Aerial Lidar observations with terrestrial lidar and snow-probe transects from NASA's 2017 SnowEx Campaign. Water Resour. Res. 55 (7), 6285–6294. https://doi.org/10.1029/2018WR024533.

Deems, J.S., Painter, T.H., Finnegan, D.C., 2013. Lidar measurement of snow depth: a review. J. Glaciol. 59 (215), 467–479. https://doi.org/10.3189/2013JoG12J154.

Dickerson-Lange, S.E., Lutz, J.A., Martin, K.A., Raleigh, M.S., Gersonde, R., Lundquist, J. D., 2015. Evaluating observational methods to quantify snow duration under diverse forest canopies. Water Resour. Res. 51 (2), 1203–1224. https://doi.org/10.1002/2014WR015744.

Egli, L., 2008. Spatial variability of new snow amounts derived from a dense network of Alpine automatic stations. Ann. Glaciol. 49, 51–55. https://doi.org/10.3189/172756408787814843.

Einhorn, B., Eckert, N., Chaix, C., Ravanel, L., Deline, P., Gardent, M., Boudières, V., Richard, D., Vengeon, J.M., Giraud, G., Schoeneich, P., 2015. Climate change and natural hazards in the Alps. Journal of Alpine Research 103-2. https://doi.org/10.4000/rga.2878.

Ellis, C.R., Pomeroy, J.W., Essery, R.L.H., Link, T.E., 2011. Effects of needleleaf forest cover on radiation and snowmelt dynamics in the Canadian Rocky Mountains. Can. J. For. Res. 41 (3), 608–620. https://doi.org/10.1139/X10-227.

Elsasser, H., Bürki, R., 2002. Climate change as a threat to tourism in the Alps. Climate Research 20, 253–257. https://doi.org/10.3354/cr020253.

Erbs, D.G., Klein, S.A., Duffie, J.A., 1982. Estimation of the diffuse radiation fraction for hourly, daily and monthly-average global radiation. Sol. Energy 28 (4), 293–302. https://doi.org/10.1016/0038-092X(82)90302-4.

Essery, R., Rutter, N., Pomeroy, J., Baxter, R., Stähli, M., Gustafsson, D., Barr, A., Bartlett, P., Elder, K., 2009. SNOWMIP2: an evaluation of forest snow process simulations. Bull. Am. Meteorol. Soc. 90 (8), 1120–1136. https://doi.org/10.1175/2009BAMS2629.1.

Farinotti, D., Usselmann, S., Huss, M., Bauder, A., Funk, M., 2012. Runoff evolution in the Swiss Alps: Projections for selected high-alpine catchments based on ENSEMBLES scenarios. Hydrol. Process. 26 (13), 1909–1924. https://doi.org/10.1002/hyp.8276.

Ferraz, A., Saatchi, S., Bormann, K., Painter, T., 2018. Fusion of NASA Airborne Snow Observatory (ASO) Lidar time series over Mountain Forest landscapes. Remote Sens. 10 (2), 164. https://doi.org/10.3390/rs10020164.

Golding, D.L., Swanson, R.H., 1986. Snow distribution patterns in clearings and adjacent forest. Water Resour. Res. 22 (13), 1931–1940. https://doi.org/10.1029/WR022i013p01931.

Goodwin, N.R., Coops, N.C., Culvenor, D.S., 2006. Assessment of forest structure with airborne LiDAR and the effects of platform altitude. Remote Sens. Environ. 103 (2), 140–152. https://doi.org/10.1016/j.rse.2006.03.003.

Grünewald, T., Schirmer, M., Mott, R., Lehning, M., 2010. Spatial and temporal variability of snow depth and ablation rates in a small mountain catchment. Cryosphere 4 (2), 215–225. https://doi.org/10.5194/tc-4-215-2010.

Harder, P., Pomeroy, J.W., Helgason, W.D., 2020. Improving sub-canopy snow depth mapping with unmanned aerial vehicles: Lidar versus structure-from-motion techniques. Cryosphere 14 (6), 1919–1935. https://doi.org/10.5194/tc-14-1919-2020.

Hardy, J.P., Melloh, R., Koenig, G., Marks, D., Winstral, A., Pomeroy, J.W., Link, T., 2004. Solar radiation transmission through conifer canopies. Agric. For. Meteorol. 126 (3), 257–270. https://doi.org/10.1016/j.agrformet.2004.06.012.

Harpold, A.A., Guo, Q., Molotch, N., Brooks, P.D., Bales, R., Fernandez-Diaz, J.C., Musselman, K.N., Swetnam, T.L., Kirchner, P., Meadows, M.W., Flanagan, J., Lucas, R., 2014. LiDAR-derived snowpack data sets from mixed conifer forests across the Western United States. Water Resour. Res. 50 (3), 2749–2755. https://doi.org/10.1002/2013WR013935.

Hedstrom, N.R., Pomeroy, J.W., 1998. Measurements and modelling of snow interception in the boreal forest. Hydrol. Process. 12 (10−11), 1611–1625. https://doi.org/10.1002/(SICI)1099-1085(199808/09)12:10/11<1611::AID-HYP684>3.0.CO;2-4.

Hojatimalekshah, A., Uhlmann, Z., Glenn, N.F., Hiemstra, C.A., Tennant, C.J., Graham, J. D., Spaete, L., Gelvin, A., Marshall, H.-P., McNamara, J.P., Enterkine, J., 2021. Tree canopy and snow depth relationships at fine scales with terrestrial laser scanning. Cryosphere 15 (5), 2187–2209. https://doi.org/10.5194/tc-15-2187-2021.

Hopkinson, C., Pomeroy, J., Debeer, C., Ellis, C., Anderson, A., 2012. Relationships between snowpack depth and primary LiDAR point cloud derivatives in a mountainous environment. IAHS Publ. 352, 354–358.

Hopkinson, C., Sitar, M., Chasmer, L., Treitz, P., 2004. Mapping snowpack depth beneath Forest Canopies using Airborne Lidar. Photogramm. Eng. Remote Sens. 70 (3), 323–330. https://doi.org/10.14358/PERS.70.3.323.

Hotovy, O., Jenicek, M., 2020. The impact of changing subcanopy radiation on snowmelt in a disturbed coniferous forest. Hydrol. Process. 34, 5298–5314. https://doi.org/10.1002/hyp.13936.

Hunziker, M., von Lindern, E., Bauer, N., Frick, J., 2012. Das Verhältnis der Schweizer Bevölkerung zum Wald. Waldmonitoring soziokulturell: Weiterentwicklung und zweite Erhebung – WaMos 2. *Birmensdorf, Eidg. Forschungsanstalt für Wald, Schnee und Landschaft WSL. 180 S*.

Hyyppä, H, Yu, X., Hyyppä, J., Kaartinen, H., Honkavaara, E., Kaasalainen, S., Rönnholm, P., 2005. Factors affecting the quality of DTM generation in forested areas. Proceedings of the ISPRS Workshop Laser scanning 2005 36, 85–90.

Jacobs, J.M., Hunsaker, A.G., Sullivan, F.B., Palace, M., Burakowski, E.A., Herrick, C., Cho, E., 2021. Snow depth mapping with unpiloted aerial system lidar observations: a case study in Durham, New Hampshire, United States. Cryosphere 15 (3), 1485–1500. https://doi.org/10.5194/tc-15-1485-2021.

Javadinejad, S., Dara, R., Jafary, F., 2020. Climate change scenarios and effects on snowmelt runoff. Civil Eng. J. 6 (9), 1715–1725. https://doi.org/10.28991/cej-2020-03091577.

Jonas, T., Essery, R., 2011. Snow cover and snowmelt in forest regions. In: Singh, V.P., Singh, P., Haritashya, U.K. (Eds.), Encyclopedia of Earth Sciences Series. Encyclopedia of Snow, Ice and Glaciers, pp. 1033–1036. https://doi.org/10.1007/978-90-481-2642-2_499. 4.

Jonas, T., Webster, C., Mazzotti, G., Malle, J., 2020. HPEval: a canopy shortwave radiation transmission model using high-resolution hemispherical images. Agric. For. Meteorol. 284, 107903 https://doi.org/10.1016/j.agrformet.2020.107903.

Kim, R.S., Durand, M.T., Li, D., Baldo, E., Margulis, S.A., Dumont, M., Morin, S., 2017. Estimating snow depth of alpine snowpack via airborne multifrequency passive microwave radiance observations: Colorado, US. AGU Fall Meeting Abstracts C13C-0983. https://ui.adsabs.harvard.edu/abs/2017AGUFM.C13C0983K.

Kostadinov, T.S., Schumer, R., Hausner, M., Bormann, K.J., Gaffney, R., McGwire, K., Painter, T.H., Tyler, S., Harpold, A.A., 2019. Watershed-scale mapping of fractional snow cover under conifer forest canopy using lidar. Remote Sens. Environ. 222, 34–49. https://doi.org/10.1016/j.rse.2018.11.037.

Koutantou, K., Mazzotti, G., Brunner, P., 2021. UAV-based lidar high-resolution snow depth mapping in the swiss Alps: comparing flat and steep forests. In: The International Archives of the Photogrammetry, Remote Sensing and Spatial Information Sciences, *XLIII-B3–2021*, pp. 477–484. https://doi.org/10.5194/isprs-archives-XLIII-B3-2021-477-2021.

LAStools, Academic Version 190812, 2019. Licensed.

Lehning, M., Grünewald, T., Schirmer, M., 2011. Mountain snow distribution governed by an altitudinal gradient and terrain roughness. Geophys. Res. Lett 38, L19504. https://doi.org/10.1029/2011GL048927.

Luce, C.H., Tarboton, D.G., 2004. The application of depletion curves for parameterization of subgrid variability of snow. Hydrol. Process. 18 (8), 1409–1422. https://doi.org/10.1002/hyp.1420.

Lundquist, J.D., Dickerson-Lange, S.E., Lutz, J.A., Cristea, N.C., 2013. Lower forest density enhances snow retention in regions with warmer winters: a global framework developed from plot-scale observations and modeling: Forests and Snow Retention. Water Resour. Res. 49 (10), 6356–6370. https://doi.org/10.1002/wrcr.20504.

MacKay, M.D., Bartlett, P.A., 2006. Estimating canopy snow unloading timescales from daily observations of albedo and precipitation. Geophys. Res. Lett. 33 (19) https://doi.org/10.1029/2006GL027521.

Malle, J., Rutter, N., Mazzotti, G., Jonas, T., 2019. Shading by trees and fractional snow cover control the subcanopy radiation budget. J. Geophys. Res. Atmos. 124 (6), 3195–3207. https://doi.org/10.1029/2018JD029908.

Mazzotti, G., Currier, W.R., Deems, J.S., Pflug, J.M., Lundquist, J.D., Jonas, T., 2019a. Revisiting snow cover variability and canopy structure within forest stands: insights from airborne lidar data. Water Resour. Res. 55 (7), 6198–6216. https://doi.org/10.1029/2019WR024898.

Mazzotti, G., Malle, J., Barr, S., Jonas, T., 2019b. Spatially continuous characterization of forest canopy structure and subcanopy irradiance derived from handheld radiometer surveys. J. Hydrometeorol. 20 (7), 1417–1433. https://doi.org/10.1175/JHM-D-18-0158.1.

Mazzotti, G., Essery, R., Moeser, C.D., Jonas, T., 2020a. Resolving small-scale forest snow patterns using an energy balance snow model with a one-layer Canopy. Water Resour. Res. 56 (1) https://doi.org/10.1029/2019WR026129.

Mazzotti, G., Essery, R., Webster, C., Malle, J., Jonas, T., 2020b. Process-level evaluation of a hyper-resolution forest snow model using distributed multisensor observations. Water Resour. Res. 56 (9) https://doi.org/10.1029/2020WR027572 e2020WR027572.

Mazzotti, G., Webster, C., Essery, R., Jonas, T., 2021. Increasing the physical representation of forest-snow processes in coarse-resolution models: lessons learned from upscaling hyper-resolution simulations. Water Resour. Res. 57 (5) https://doi.org/10.1029/2020WR029064.

Moeser, D., Stähli, M., Jonas, T., 2015. Improved snow interception modeling using canopy parameters derived from airborne LiDAR data. Water Resour. Res. 51 (7), 5041–5059. https://doi.org/10.1002/2014WR016724.

Moeser, C.D., Broxton, P.D., Harpold, A., Robertson, A., 2020. Estimating the effects of forest structure changes from wildfire on snow water resources under varying meteorological conditions. Water Resour. Res. 56 (11) https://doi.org/10.1029/2020WR027071.

Mott, R., Vionnet, V., Grünewald, T., 2018. The seasonal snow cover dynamics: review on wind-driven coupling processes. Front. Earth Sci. 6, 197. https://doi.org/10.3389/feart.2018.00197.

Musselman, K.N., Pomeroy, J.W., Link, T.E., 2015. Variability in shortwave irradiance caused by forest gaps: Measurements, modelling, and implications for snow energetics. Agric. For. Meteorol. 207, 69–82. https://doi.org/10.1016/j.agrformet.2015.03.014.

Nöthiger, C., Elsasser, H., 2004. Natural hazards and tourism: new findings on the European Alps. Mt. Res. Dev. 24 (1), 24–27. https://doi.org/10.1659/0276-4741(2004)024[0024:NHATNF]2.0.CO;2.

Painter, T.H., Berisford, D.F., Boardman, J.W., Bormann, K.J., Deems, J.S., Gehrke, F., Hedrick, A., Joyce, M., Laidlaw, R., Marks, D., Mattmann, C., McGurk, B., Ramirez, P., Richardson, M., Skiles, S.M., Seidel, F.C., Winstral, A., 2016. The airborne snow observatory: Fusion of scanning lidar, imaging spectrometer, and physically-based modeling for mapping snow water equivalent and snow albedo. Remote Sens. Environ. 184, 139–152. https://doi.org/10.1016/j.rse.2016.06.018.

Perrot, D., Pugh, E.T., Molotch, N.P., Small, E.E, 2011. Effects of forest litter and aeolian dust deposition on snow surface albedo. AGU Fall Meet. Abstr. B33B-0458.

Raleigh, M.S., Small, E.E., 2017. Snowpack density modeling is the primary source of uncertainty when mapping basin-wide SWE with lidar. Geophys. Res. Lett. 44 (8), 3700–3709. https://doi.org/10.1002/2016GL071999.

Riaño, D., Chuvieco, E., Ustin, S.L., Salas, J., Rodríguez-Pérez, J.R., Ribeiro, L.M., Viegas, D.X., Moreno, J.M., Fernández, H., 2007. Estimation of shrub height for fuel-type mapping combining airborne LiDAR and simultaneous color infrared ortho imaging. Int. J. Wildland Fire 16 (3), 341. https://doi.org/10.1071/WF06003.

Rixen, C., Teich, M., Lardelli, C., Gallati, D., Pohl, M., Pütz, M., Bebi, P., 2011. Winter tourism and climate change in the Alps: an assessment of resource consumption, snow reliability, and future snowmaking potential. Mt. Res. Dev. 31 (3), 229–236. https://doi.org/10.1659/MRD-JOURNAL-D-10-00112.1.

Safa, H., Krogh, S.A., Greenberg, J., Kostadinov, T.S., Harpold, A.A., 2021. Unraveling the controls on snow disappearance in montane conifer forests using multi-site lidar. Water Resour. Res. 57 https://doi.org/10.1029/2020WR027522 e2020WR027522.

Schirmer, M., Pomeroy, J.W., 2020. Processes governing snow ablation in alpine terrain – detailed measurements from the Canadian Rockies. Hydrol. Earth Syst. Sci. 24 (1), 143–157. https://doi.org/10.5194/hess-24-143-2020.

Spaete, L.P., Glenn, N.F., Derryberry, D.R., Sankey, T.T., Mitchell, J.J., Hardegree, S.P., 2011. Vegetation and slope effects on accuracy of a LiDAR-derived DEM in the sagebrush steppe. Remote Sens. Lett. 2 (4), 317–326. https://doi.org/10.1080/01431161.2010.515267.

Streutker, D.R., Glenn, N.F., 2006. LiDAR measurement of sagebrush steppe vegetation heights. Remote Sens. Environ. 102 (1), 135–145. https://doi.org/10.1016/j.rse.2006.02.011.

Su, J., Bork, E., 2006. Influence of vegetation, slope, and lidar sampling angle on DEM accuracy. Photogramm. Eng. Remote Sens. 72 (11), 1265–1274. https://doi.org/10.14358/PERS.72.11.1265.

Thornton, J.M., Brauchli, T., Mariethoz, G., Brunner, P., 2021. Efficient multi-objective calibration and uncertainty analysis of distributed snow simulations in rugged alpine terrain. J. Hydrol. 598, 126241 https://doi.org/10.1016/j.jhydrol.2021.126241.

Tinkham, W.T., Smith, A.M.S., Hoffman, C., Hudak, A.T., Falkowski, M.J., Swanson, M. E., Gessler, P.E., 2012. Investigating the influence of LiDAR ground surface errors on the utility of derived forest inventories. Can. J. For. Res. 42 (3), 413–422. https://doi.org/10.1139/x11-193.

Trujillo, E., Ramírez, J.A., Elder, K.J., 2007. Topographic, meteorologic, and canopy controls on the scaling characteristics of the spatial distribution of snow depth fields: spatial scaling of snow depth. Water Resour. Res. 43 (7) https://doi.org/10.1029/2006WR005317.

Uhlmann, Z., Glenn, N.F., Spaete, L.P., Hiemstra, C., Tennant, C., McNamara, J., 2018. Resolving the influence of forest-canopy structure on snow depth distributions with terrestrial laser scanning. In: IGARSS 2018–2018 IEEE International Geoscience and

Remote Sensing Symposium, pp. 6284–6286. https://doi.org/10.1109/IGARSS.2018.8517911.

Vander Jagt, B., Lucieer, A., Wallace, L., Turner, D., Durand, M., 2015. Snow depth retrieval with UAS using photogrammetric techniques. Geosciences 5 (3), 264–285. https://doi.org/10.3390/geosciences5030264.

Webb, R.W., Raleigh, M.S., McGrath, D., Molotch, N.P., Elder, K., Hiemstra, C., Brucker, L., Marshall, H.P., 2020. Within-stand boundary effects on snow water equivalent distribution in forested areas. Water Resour. Res. 56 (10) https://doi.org/10.1029/2019WR024905 e2019WR024905.

Webster, C., Rutter, N., Zahner, F., Jonas, T., 2016. Modeling subcanopy incoming longwave radiation to seasonal snow using air and tree trunk temperatures: Modeling Subcanopy Longwave Radiation. J. Geophys. Res. Atmos. 121 (3), 1220–1235. https://doi.org/10.1002/2015JD024099.

Webster, C., Rutter, N., Jonas, T., 2017. Improving representation of canopy temperatures for modeling subcanopy incoming longwave radiation to the snow surface. J. Geophys. Res. Atmos. 122 (17), 9154–9172. https://doi.org/10.1002/2017JD026581.

Webster, C., Mazzotti, G., Essery, R., Jonas, T., 2020. Enhancing airborne LiDAR data for improved forest structure representation in shortwave transmission models. Remote Sens. Environ. 249, 112017 https://doi.org/10.1016/j.rse.2020.112017.

Wipf, S., Stoeckli, V., Bebi, P., 2009. Winter climate change in alpine tundra: Plant responses to changes in snow depth and snowmelt timing. Clim. Chang. 94 (1–2), 105–121. https://doi.org/10.1007/s10584-009-9546-x.

YellowScan CloudStation, 2021. Version 1.18.0, Licensed.

Zheng, Z., Kirchner, P.B., Bales, R.C., 2016. Topographic and vegetation effects on snow accumulation in the southern Sierra Nevada: a statistical summary from lidar data. Cryosphere 10 (1), 257–269. https://doi.org/10.5194/tc-10-257-2016.

Zheng, Z., Ma, Q., Qian, K., Bales, R., 2018. Canopy effects on snow accumulation: observations from Lidar, canonical-view photos, and continuous ground measurements from sensor networks. Remote Sens. 10 (11), 1769. https://doi.org/10.3390/rs10111769.